

ORIGINAL RESEARCH

Open Access



# Application of a simplified Grey Wolf optimization technique for adaptive fuzzy PID controller design for frequency regulation of a distributed power generation system

Sasmita Padhy\* and Sidhartha Panda

## Abstract

A Simplified Grey Wolf Optimizer (SGWO) is suggested for resolving optimization tasks. The simplification in the original Grey Wolf Optimizer (GWO) method is introduced by ignoring the worst category wolves while giving priority to the better wolves during the search process. The advantage of the presented SGWO over GWO is a better solution taking less execution time and is demonstrated by taking unimodal, multimodal, and fixed dimension test functions. The results are also contrasted to the Gravitational Search Algorithm, the Particle Swarm Optimization, and the Sine Cosine Algorithm and this shows the superiority of the proposed SGWO technique. Practical application in a Distributed Power Generation System (DPGS) with energy storage is then considered by designing an Adaptive Fuzzy PID (AFPID) controller using the suggested SGWO method for frequency control. The DPGS contains renewable generation such as photovoltaic, wind, and storage elements such as battery and flywheel, in addition to plug-in electric vehicles. It is demonstrated that the SGWO method is superior to the GWO method in the optimal controller design task. It is also seen that SGWO based AFPID controller is highly efficacious in regulating the frequency compared to the standard PID controller. A sensitivity study is also performed to examine the impact of the unpredictability in the parameters of the investigated system on system performance. Finally, the novelty of the paper is demonstrated by comparing with the existing publications in an extensively used two-area test system.

**Keywords:** Frequency control, Distributed power generation system, Adaptive fuzzy PID controller, Grey wolf optimization, Electric vehicle

## 1 Introduction

The Grey Wolf Optimizer (GWO) is a new optimization method applied to diversified objectives in different optimization tasks. Because of its comprehensibility, high flexibility, and quick programmability features [1], and dealing with fewer algorithm parameters, it has attracted significant research interests from numerous fields over a short time [2, 3]. The performance of the GWO can be

enhanced by maintaining an equilibrium amongst the exploration and exploitation stages in the course of searching. A lot of effort has been put in to modify the GWO to improve its performance on optimization problems [4–7]. However, modifications of the original GWO method to enhance its versatility increase its complexity. To address such issues, this study simplifies the original GWO method as proposed in [8, 9]. In the original GWO, four categories of grey wolves, namely alpha ( $\alpha$ ), beta ( $\beta$ ), delta ( $\delta$ ), and omega ( $\omega$ ) are engaged in mimicking the

\* Correspondence: [sasmitapadhy@ieee.org](mailto:sasmitapadhy@ieee.org)  
Department of Electrical Engineering, VSSUT, Burla, Odisha 768018, India

leadership ladder and equal importance is given to the alpha, beta and delta wolves to compute the updated position of wolves throughout the iterations. In the proposed Simplified GWO (SGWO), the least fit wolves, i.e., the delta wolves, are eliminated and more importance is attached to the  $\alpha$  wolves to find updated positions. This not only reduces the complexity and improves the execution time but also improves the solution quality.

In most countries, the majority of electricity supplies are through centralized power plants [10, 11]. This results in problems such as high power loss during transmission and distribution, deficiencies in the power grid, unreliable power supply, etc. In addition, there is a lack of flexibility in conventional centralized electricity generation to adjust to the challenges posed by recent changes in energy consumption. Hence a clear shift can be observed from a centralized system to a decentralized mode [12, 13]. To satisfy the demand of an isolated community, the expansion of DER (Distributed Energy Resources) can be done by interconnection with storage devices [14–17]. The probabilistic characteristics of wind and solar sources and random demand create power imbalance and produce frequency oscillation. To overcome these challenges, an intelligent and flexible secondary controller is needed one which can operate in any situations with reduced settling time and oscillation. Therefore, for a Distributed Power Generation System (DPGS) which includes distributed energy resources and energy storage systems, an algorithm which can improve system response and thereby prevent system collapse is essential.

Previous work has shown that effective frequency regulation of the DPGS system is dependent on controller design and the practice used to select the control parameters and gains. Numerous methodologies have been proposed to design the controller gains, e.g., optimal controller [18], Genetic Algorithm (GA) [19], Particle Swarm Optimization (PSO) [20], Differential Evolution (DE) [21], Teaching Learning Based Optimization (TLBO) [22], Gravitational Search Algorithm (GSA) [23], Cuckoo Search (CS) algorithm [24], BAT algorithm (BAT) [25], MWOA [26], SCA [27] etc. The Jaya algorithm in [28] optimizes PID parameters for frequency control of a power system with renewable sources, while the Electro Search Optimization (ESO) algorithm [29] with balloon effect is proposed to control the frequency of an isolated power system.

Classical controllers may not provide the desired performance for systems containing nonlinearity and constraints [30, 31]. Conversely, a Fuzzy Logic Controller (FLC) enhances the attainment of PID structure and can handle nonlinearity and uncertainty. Depending on the choice of Scaling Factors (SFs) engaged in input/output and the controller gains, an FLC can be designed [32]. On some occasions, straight forward FLC approaches

are not enough to produce the required control actions. In this instance, the controller structure of the FLC can be modified to make it adaptive [33, 34]. This paper proposes an Adaptive Fuzzy PID (AFPID) structure that receives the input signal and appropriately changes the output control signal.

The main contributions are:

1. A Simplified GWO (SGWO) approach is proposed to adjust the AFPID parameters of a DPGS for frequency regulation.
2. The advantage of the proposed SGWO over GWO is established by taking several unimodal and multimodal standard functions.
3. The SGWO strategy is deployed to adjust the parameters of an AFPID controller and the outcomes are correlated with the SGWO tuned PID controller in a real engineering problem.
4. Frequency variations, control signals, and power responses of individual regulated sources of the DPGS are examined with established PID and AFPID controllers.
5. A sensitivity study is performed to prove the robustness of AFPID by introducing variability to parameters of the DPGS. The consequence of uncertainties on DPGS due to AFPID and PID controllers are demonstrated by considering some serious scenarios.

## 2 System modeling

The proposed SGWO method is tested for tuning of the adaptive fuzzy PID controller to reduce frequency deviation in a DPGS as illustrated in Fig. 1 [34]. The DPGS system in Fig. 1 contains sources such as WTG (Wind Turbine Generator), PV (Solar Photovoltaic), AE (Aqua Electrolysers), an FC (Fuel-cell), a DEG (Diesel Engine Generator), a FESS (Flywheel Energy Storage System), a BESS (Battery Energy Storage System), an EV (Electric Vehicle), etc. In Fig. 1, the different elements for generation of power (WTG, PV, FC, DEG) and storage of power (BESS, FESS, and EV) are represented by appropriate transfer functions. Sixty percent of the power generated from the WTG and PV are used for producing the source power and the remaining 40% is used by the AE to make hydrogen for the FC. The dynamic characteristic of the DPGS system is highly erratic as the renewable power outputs rely on climatic conditions. For all the subsystems considered in the DPGS, a centralized controller is implemented instead of many controllers. This results in low maintenance, simple control, and design flexibility with fewer control variables. Communication delays for the signals to reach the controller and for receiving the control signals from the controller are considered. To obtain an acceptable time domain signal

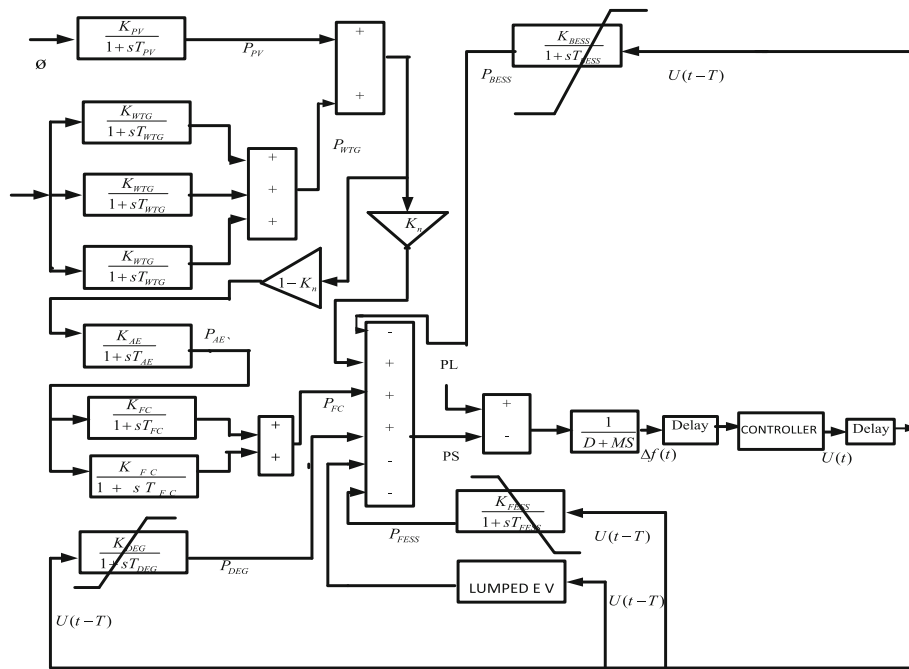


**Fig. 1** Hybrid power system under study

with reduced settling time and oscillation, the signals are modified by rate limiters according to the electromechanical characteristics of individual elements presented in the distributed power network as shown in Fig. 4.

A. Wind turbine generator

The power produced by three WTGs in Fig. 1 is represented by  $P_{WP}$ . It depends upon density of air ( $\rho$ ), velocity of wind ( $V_W$ ), wind turbine’s blade swept area ( $A_R$ ), and is given as:

$$P_{WP} = \frac{1}{2} \rho A_R C_P V_W^3 \tag{1}$$

where  $C_P$  is the power coefficient.

The wind turbine system has numerous nonlinearities including the pitch system. Change in the pitch angle introduces nonlinearity into the wind turbine.

The WTG transfer function (T/F) is given as:

$$G_{WTGN}(s) = \frac{K_{WTG}}{1 + sT_{WTG}} = \frac{\Delta P_{WTG}}{\Delta P_{WP}} \tag{2}$$

Where  $N = 1, 2, 3$  represents the number of WT units.  $K_{WTG}$  and  $T_{WTG}$  are the gain and the time constant. In (2), the change of wind power is the input to the wind turbine and the change in the power of the wind turbine generator is the output.

B. Photovoltaic cell

The photovoltaic power ( $P_{PV}$ ) equation is specified by:

$$P_{PV} = \eta \cdot S \cdot \phi [1 - 0.005(T_a + 25)] \tag{3}$$

where  $S$  is the area of the PV array taken as  $4084m^2$ ,  $\eta$  is the conversion efficiency of PV cells taken as 10%, and  $\phi$  is the solar irradiation in  $kW/m^2$ . The PV system T/F is specified by:

$$G_{PV}(s) = \frac{K_{PV}}{1 + sT_{PV}} = \frac{\Delta P_{PV}}{\Delta \phi} \tag{4}$$

The change in Solar irradiation is the input to the PV cell and output is the change in generated PV cell power.

C. Aqua electrolyzer

The aqua electrolyzer gets a significant proportion of the net power produced by wind and PV cells. It produces for FC power generation. The AE TF is given as

$$G_{AE}(s) = \frac{K_{AE}}{1 + sT_{AE}} = \frac{\Delta P_{AE}}{U_2} \tag{5}$$

D. Fuel cell

The FC plays a major role as it is clear and has high efficiency. The fuel cell generator is a higher-order system but for low frequency, the 1st order T/F is taken as:

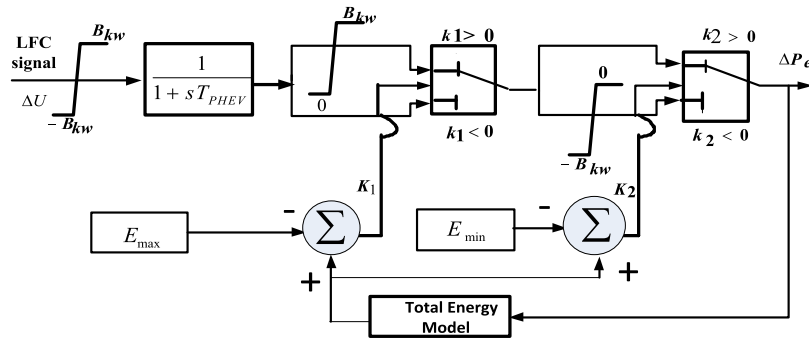


**Fig. 2** Modeling of one electric vehicle

$$G_{FCN}(s) = \frac{K_{FC}}{1 + sT_{FC}} = \frac{\Delta P_{FC}}{\Delta P_{AE}} \quad (6)$$

$N = 1, 2$  for two units.

E. Diesel engine generator

The (DEG) can supply the deficiency power to minimize the power disparity among demand and supply. It is a nonlinear element as it has generation restrictions. Its T/F is given as:

$$G_{DEG}(s) = \frac{K_{DEG}}{1 + sT_{DEG}} = \frac{\Delta P_{DEG}}{\Delta U} \quad (7)$$

F. Energy storage system modelling

The energy storage elements are controlled by the controller output signal. As needed, they perform as sources or loads to the system. They include rate restrictions which let the elements function in the nonlinear region. In addition,

the rate constraints help to deal with the electromechanical features shown by the devices and prevent a mechanical blow caused by sudden frequency variations. These nonlinearities and limits are given by  $|P_{FESS} \dot{< 0.09|, |P_{BESS} \dot{< 0.09|, |P_{DEG} \dot{< 0.01|, |P_{EV} \dot{< 0.01|, |P_{FESS} \dot{< 0.9|, |P_{BESS} \dot{< 0.2|, |P_{EV} \dot{< 0.5|}$  and  $0 \leq P_{DEG} \leq 0.45$ .

This will avoid any element to rapidly discharging or accumulating energy. The T/F of the FESS is given as:

$$G_{FESS}(s) = \frac{K_{FESS}}{1 + sT_{FESS}} = \frac{\Delta P_{FESS}}{\Delta U} \quad (8)$$

The transfer function of the BESS is given as:

$$G_{BESS} = \frac{K_{BESS}}{1 + sT_{BESS}} = \frac{\Delta P_{BESS}}{\Delta U} \quad (9)$$

G. Electric vehicle (EV) modelling

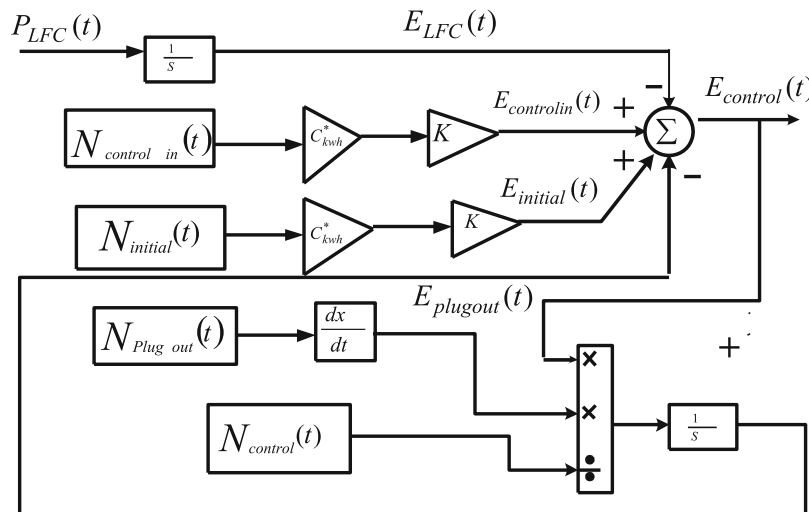


**Fig. 3** Total energy model of one EV

The block diagram representation of EV for frequency regulation is shown in Fig. 2. The LFC signal  $\Delta U$  is given to the EV which receives/gives the real power throughout charging/discharging. The variable  $\pm BkW$  indicates the battery capacity and  $T_{PHEV}$  is the time constant of an EV. The present battery energy is represented by  $E$  which is regulated between limits  $E_{max}$  and  $E_{min}$  assumed as 90% and 80% of the rated energy, respectively.  $K_1$  and  $K_2$  are the energy mismatch given as  $K_1 = E - E_{max}$  and  $K_2 = E - E_{min}$ .

In Fig. 1, the group of EVs which are ready to contribute power to the grid are engaged as a lumped model for the frequency control scheme. In addition, the LFC signal is sent to the EVs according to their state of charge (SOC) for charging or discharging purpose. Afterward the SOC of the EVs is synchronized. In order for the EV to operate in an LFC strategy, dissemination of information among the EV and power system is necessary. In this paper the LC (local control) centers act as the link between the central load dispatching center (CLDC) and the EV. The LFC signal is directed by the CLDC to the EV and the actual states such as power available in the EV, inverter capacity and amount of SOC from the EV are dispatched to the CLDC by means of the LC centers. CLDC computes the LFC signal from the frequency variation and determines the involvement of the EV in the LFC. The charging and discharging of the EV count on its SOC while SOC is vastly reliant on the LFC signal which CLDC dispatches. When the SOC hits the limiting values, the EV stops participating in LFC. The model for the energy stored in one EV is illustrated in Fig. 3. At instant  $t$ , the quantity of controllable EVs,  $N_{controllable}(t)$  taking part in the AGC is determined from statistics of the original quantity of controllable EVs at the start of the interval that stop participating in the LFC. The total energy model in Fig. 3 finds the remaining stored battery energy in an LC center as in [15]. The model for the energy stored in one EV is illustrated in Fig. 3.

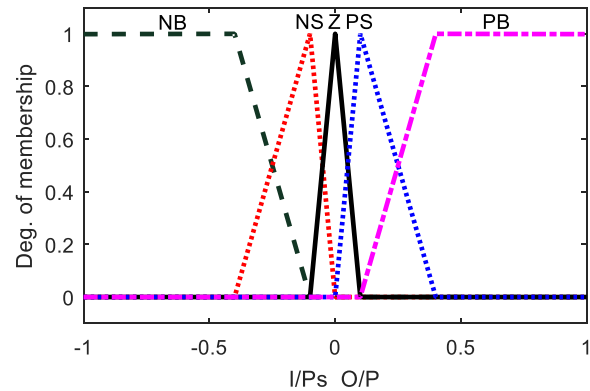


**Fig. 5** Membership function of error and change of error of AFLC

At time  $t$ , the quantity of controllable EVs  $N_{controllable}(t)$  taking part in AGC are determined from statistics of the original quantity of controllable EVs at the start of the interval  $(N_{initial}(t) - N_{plugout}(t))$  gives the EV number shifting from controllable condition to driving condition in that time while  $N_{controlin}(t)$  gives the EV number shifting from charging condition to controllable condition. Thus,  $N_{controllable}(t)$  can be obtained as:

$$N_{controllable}(t) = N_{initial}(t) - N_{plugout}(t) + N_{controlin}(t) \tag{10}$$

The expression for the energy is given as:

$$E_{control}(t) = E_{initial}(t) + E_{controlin}(t) - E_{plugout} - E_{LFC}(t) \tag{11}$$

$E_{controlin}(t)$  can be written as

$$E_{controlin}(t) = C_{kWh}^* \cdot N_{controlin}(t) = 0.8B_{kW}^* \cdot N_{controlin}(t) [kWh] \tag{12}$$

In Fig. 3,  $E_{LFC}$  is the energy related to the LFC signal and is given by integrating the power of local control centre ( $P_{LFC}$ ) as:

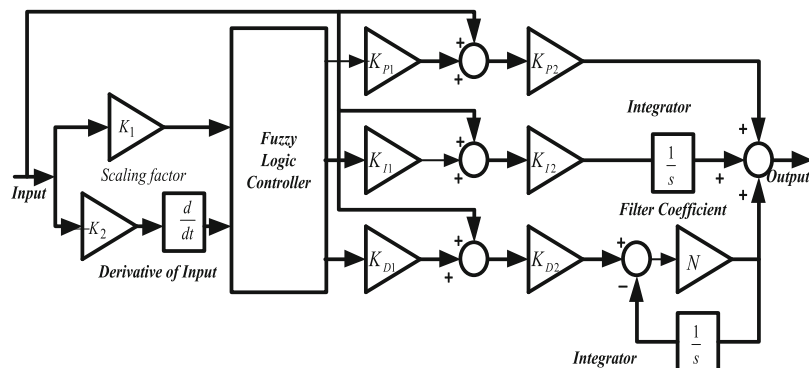


**Fig. 4** Adaptive Fuzzy PID structure

**Table 1** Comparison of proposed SGWO with other techniques for unimodal benchmark test functions

F	SCA		PSO		GSA		GWO		SGWO	
	Avg.	Std. Dev	Avg.	Std. Dev						
$f_1$	18.0038	42.5623	0.000136	0.000202	2.53E-16	9.67E-17	6.59E-28	6.34E-5	<b>4.07E-32</b>	<b>1.510E-31</b>
$f_2$	0.0178	0.0215	0.042144	0.045421	0.055655	0.194074	7.18E-17	0.029014	<b>9.477E-20</b>	<b>1.239E-19</b>
$f_3$	8.0222E3	5.8196E3	70.12562	22.11924	896.5347	318.9559	3.29E-06	7.91495E-5	<b>8.97E-8</b>	<b>2.407E-7</b>
$f_4$	34.5259	12.0554	1.086481	0.317039	7.35487	1.741452	5.61E-07	1.315088	<b>9.78E-8</b>	<b>1.289E-7</b>
$f_5$	1.0104E5	3.7340E5	96.71832	60.11559	67.54309	62.22534	26.81258	0.8028	26.7796	0.5535
$f_6$	18.8163	26.9175	0.000102	8.28E-05	2.5E-16	1.74E-16	0.816579	0.3437	0.9256	0.2949
$f_7$	0.1218	0.0995	0.122854	0.044957	0.089441	0.04339	0.002213	0.10028	<b>0.0016</b>	<b>0.0009</b>

$$E_{LFC}(t) = \int_0^t P_{LFC}(t)dt \tag{13}$$

H. Power system modelling

The dynamics of the power system with the change in power ( $\Delta P$ ) as input and the change in frequency ( $\Delta f$ ) as output is given by:

$$G(s) = \frac{\Delta f}{\Delta P} = \frac{1}{D + Ms} \tag{14}$$

In (14),  $D$  equals 0.03 and is the damping parameter while  $M=0.4$  is the inertia parameter of the DPGS system [20]. The relevant data are given in the appendix.

2.1 Structure of AFPID controller

Various approaches can be employed for designing FLC scheme. One approach is the online selection of membership function (MFs) where complexity increases and requires high computation. Alternatively, a PID controller can be used and its gains and input scaling factors are upgraded using optimization technique. In the first design method, the SFs remains fixed while in the other approach the SFs are chosen regularly during controller operation. However, the effectiveness of the Fuzzy PID structure could be unacceptable because of no straight

link among inputs errors to the PID. To overcome the above restrictions, Adaptive Fuzzy PID (AFPID) is planned as shown in Fig. 4.

In the AFPID, the input is processed through the FLC and is connected to the PID controllers. For the projected AFPID controller, a standard rule base and five MFs (triangular) are selected as displayed in Fig. 5.

The MFs are allocated linguistic variables Negative Big (NB), Negative Small (NS), Zero (Z), Positive Small (PS) and Positive Big (PB) for both input and output as presented later. The SFs are selected by the SGWO method. In the present study, a Mamdani fuzzy inference engine [30] is chosen. Frequency error and change in frequency error are taken as the inputs to the FLC.

2.2 Problem formulation

Minimization of frequency fluctuation ( $\Delta f$ ) along with the controller output ( $\Delta u$ ) is the objective function and can be depicted by integral square error (ISE) given as:

$$J = \int_0^T [(\Delta f)^2 + (\Delta u)^2/k]dt \tag{15}$$

where  $k$  is selected as 5 to give both parts in (15) the same weight in the course of the optimization process. The SGWO method is engaged to tune the PID gains and the SFs of the AFPID controller. The  $\Delta f$  and  $\Delta u$

**Table 2** Comparison of proposed SGWO with other techniques for multimodal benchmark test functions

F	SCA		PSO		GSA		GWO		SGWO	
	Avg.	Std. Dev	Avg.	Std. Dev	Avg.	Std. Dev	Avg.	Std. Dev	Avg.	Std. Dev
$f_8$	-3.7209E3	0.2587E3	-4841.29	1152.814	-2821.07	493.0375	-6123.1	-4087.44	<b>-5.6287E3</b>	<b>0.9503E3</b>
$f_9$	45.6190	31.4763	46.70423	11.62938	25.96841	7.470068	0.310521	47.35612	<b>0.6186</b>	<b>1.8970</b>
$f_{10}$	15.1791	8.4852	0.276015	0.50901	0.062087	0.23628	1.06E-13	0.07783E-13	<b>3.322E-14</b>	<b>5.93E-15</b>
$f_{11}$	0.9576	0.6136	0.009215	0.007724	27.70154	5.040343	0.004485	0.006659	<b>0.0025</b>	<b>0.007</b>
$f_{12}$	0.6073E5	3.0109E5	0.006917	0.026301	1.799617	0.95114	0.053438	0.020734	<b>0.0604</b>	<b>0.0329</b>
$f_{13}$	1.001E5	3.1194E5	0.006675	0.008907	8.899084	7.126241	-6123.1	-4087.44	<b>0.7567</b>	<b>0.2869</b>

**Table 3** Comparison of proposed SGWO with other techniques for fixed-dimension test functions

F	SCA		PSO		GSA		GWO		SGWO	
	Avg.	Std. Dev	Avg.	Std. Dev	Avg.	Std. Dev	Avg.	Std. Dev	Avg.	Std. Dev
$f_{14}$	2.5095	2.4449	3.6271	2.5608	5.8598	3.8313	4.042493	4.252799	<b>2.0510</b>	<b>1.9064</b>
$f_{15}$	0.9457E-3	0.3779E-3	<b>0.00057</b>	<b>0.00022</b>	0.0036	0.0016	0.0031	0.000625	0.0017	0.0051
$f_{16}$	-1.0316	0.0001	-1.03163	6.25E-16	-1.03163	4.88E-16	-1.03163	-1.03163	<b>-1.0316</b>	<b>0.0</b>
$f_{17}$	0.4009	0.0031	0.397887	0	0.3978	0	0.397889	0.397887	<b>0.3979</b>	<b>6.33E-5</b>
$f_{18}$	3.0001	0.0001	3.0	1.33E-15	3.0	4.17E-15	3.000028	3.0	3.0	1.89E-5
$f_{19}$	-3.8539	0.0018	-3.8627	2.58E-15	-3.8627	2.29E-15	-3.8622	1.4E-5	<b>-3.8609</b>	<b>3.17E-3</b>

signal have least  $J$  value for the efficient performance of the DPGS.

### 3 Simplified grey wolf optimization (SGWO)

GWO is one of the recently recommended optimization approaches which is encouraged by coursing behavior and the social ladder of grey wolves [1]. GWO has the following key steps:

1. Search the prey and approach it.
2. Encircle it and restricts its movement.
3. Kill the prey.

References [1–5] narrate the above points while in the proposed SGWO, only two categories of wolves ( $\alpha$  and  $\beta$ ) are considered while delta wolves are neglected like omega wolves in the original GWO algorithm. The updated position formula of the  $\alpha$ ,  $\beta$ , and  $\delta$  wolves around the prey during hunting in the original GWO algorithm are governed by

$$\begin{aligned} S_\alpha &= \left| \vec{C}_1 \cdot \vec{Y}_\alpha - \vec{Y} \right|, S_\beta = \left| \vec{C}_2 \cdot \vec{Y}_\beta - \vec{Y} \right| \\ S_\delta &= \left| \vec{C}_3 \cdot \vec{Y}_\delta - \vec{Y} \right| \end{aligned} \tag{16}$$

$$\begin{aligned} \vec{Y}_1 &= \vec{Y}_\alpha - \vec{A}_1 \cdot (\vec{S}_\alpha), \vec{Y}_2 = \vec{Y}_\beta - \vec{A}_1 \cdot (\vec{S}_\beta) \\ \vec{Y}_3 &= \vec{Y}_\delta - \vec{A}_1 \cdot (\vec{S}_\delta) \end{aligned} \tag{17}$$

Updated position formula of the  $\alpha$  and  $\beta$  wolves in SGWO is formulated by modifying (16) and (17) as:

$$\vec{S}_\alpha = \left| \vec{C}_1 \cdot \vec{Y}_\alpha - \vec{Y} \right|, \vec{S}_\beta = \left| \vec{C}_2 \cdot \vec{Y}_\beta - \vec{Y} \right| \tag{18}$$

$$\vec{Y}_1 = \vec{Y}_\alpha - \vec{A}_1 \cdot (\vec{S}_\alpha), \vec{Y}_2 = \vec{Y}_\beta - \vec{A}_2 \cdot (\vec{S}_\beta) \tag{19}$$

where  $\vec{Y}_\alpha, \vec{Y}_\beta, \vec{Y}_\delta$  and  $\vec{S}_\alpha, \vec{S}_\beta, \vec{S}_\delta$  are the current and updated positions of  $\alpha, \beta$  and  $\delta$  wolves respectively, and  $\vec{A}_i$  and  $\vec{C}_i$  are the coefficient vectors governing the position inside the space around the prey.

In the GWO technique, the position of a grey wolf is governed by positions of all participating wolves, i.e.  $\alpha, \beta$ , and  $\delta$  wolves irrespective of their fitness as:

$$\vec{Y}(t+1) = \frac{\vec{Y}_1 + \vec{Y}_2 + \vec{Y}_3}{3} \tag{20}$$

Being at the front rank of the group,  $\alpha$  category wolf is ahead of  $\beta$  category wolf, and the  $\delta$  category wolf is skipped in the recommended SGWO. More significance is provided to  $\alpha$  wolves positions relative to  $\beta$  wolves to

**Table 4** Comparison of computational time between GWO and SGWO for unimodal functions

Function	GWO Elapsed time (sec)	SGWO Elapsed time (sec)	% reduction in execution time
$f_1$	4.99	4.73	5.21
$f_2$	5.65	5.21	7.78
$f_3$	18.78	18.21	3.03
$f_4$	5.49	4.76	13.29
$f_5$	6.19	5.81	6.13
$f_6$	5.35	5.14	3.92
$f_7$	7.72	6.86	11.14

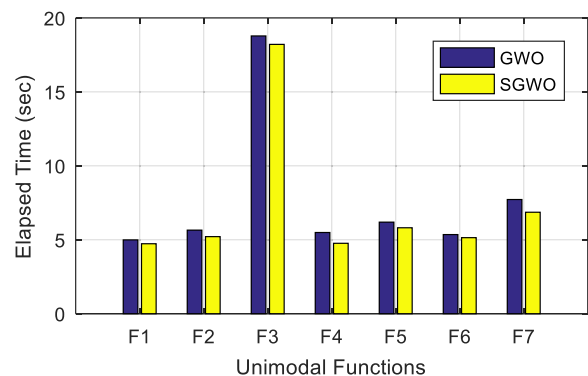


**Fig. 6** Unimodal function's Execution time comparison

**Table 5** Comparison of computational time between GWO and SGWO for multimodal functions

Function	GWO Elapsed time (sec)	SGWO Elapsed time (sec)	%% reduction in execution time
$f_8$	6.22	5.92	4.82
$f_9$	5.36	5.06	5.59
$f_{10}$	5.77	5.51	4.51
$f_{11}$	6.16	5.98	2.92
$f_{12}$	13.58	13.39	1.39
$f_{13}$	13.98	12.66	9.44

decide the position of a grey wolf in the SGWO as expressed by:

$$\vec{Y}(t+1) = \frac{2\vec{Y}_1 + \vec{Y}_2}{3} \tag{21}$$

### 4 Application of SGWO for frequency control problems

#### 4.1 Performance assessment of SGWO

Before the application of SGWO, the performance of the SGWO technique for some benchmark test functions (BTFs) is assessed. The expressions of test functions, their features, and optimized values are available in the literature [1]. While executing the SGWO algorithms the following algorithm parameters are chosen: search agents = 30, maximum iterations = 500, no. of runs = 30 as proposed in the original GWO. The statistical outcomes such as average and standard deviations as well as execution time for 30 runs are listed in Tables 1, 2, and 3 for unimodal, multimodal, and fixed dimension functions, respectively. To validate the superiority of the SGWO technique over GWO, GSA, PSO in [1] and SCA in [27], the results are compared in the tables. As is seen

**Table 6** Comparison of computational time between GWO and SGWO for fixed-dimension test functions

Function	GWO Elapsed time (sec)	SGWO Elapsed time (sec)	% reduction in execution time
$f_{14}$	27.62	26.25	4.96
$f_{15}$	2.77	2.549	7.97
$f_{16}$	1.99	1.86	6.53
$f_{17}$	1.87	1.72	8.02
$f_{18}$	1.79	1.71	4.47
	3.91	3.79	3.07

from Table 1, the SGWO technique is more powerful for unimodal functions and outperforms GWO, GSA, PSO, and SCA for 5 ( $f_1, f_2, f_3, f_4, f_7$ ) out of 7 functions.

The computational times for GWO and SGWO are given in Table 4 for all the unimodal functions. It can be seen that, for all the unimodal functions computational time is less for the SGWO than for the original GWO. For better illustration, the percentage improvements in execution times are reported in Table 4 as well as shown in Fig. 6. The corresponding equivalent outcomes of multimodal test functions are provided in Table 5 and Fig. 7. It is noticed from Table 5 that, the suggested SGWO surpasses GWO, GSA, PSO, and SCA in all multimodal test functions with reduced computational time compared to the original GWO (shown in Table 5 and Fig. 7).

The outcomes of fixed dimension functions are listed in Table 3, which clearly shows that the proposed SGWO technique outperforms GWO, GSA, PSO and SCA for 4 ( $f_{14}, f_{16}, f_{17}, f_{19}$ ) out of 6 fixed dimension test functions. For the remaining two benchmark functions, SGWO provides a more desirable outcome than GWO, GSA, and SCA for  $f_{14}$ .

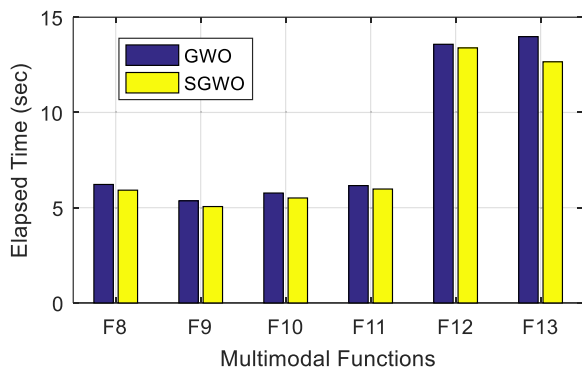


**Fig. 7** Multi-modal function’s execution time comparison of GWO and SGWO technique

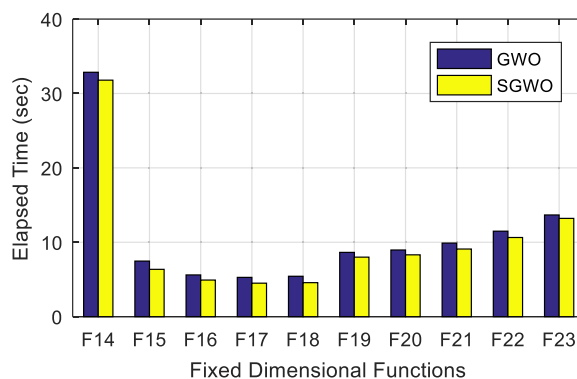


**Fig. 8** Fixed dimension function’s execution time

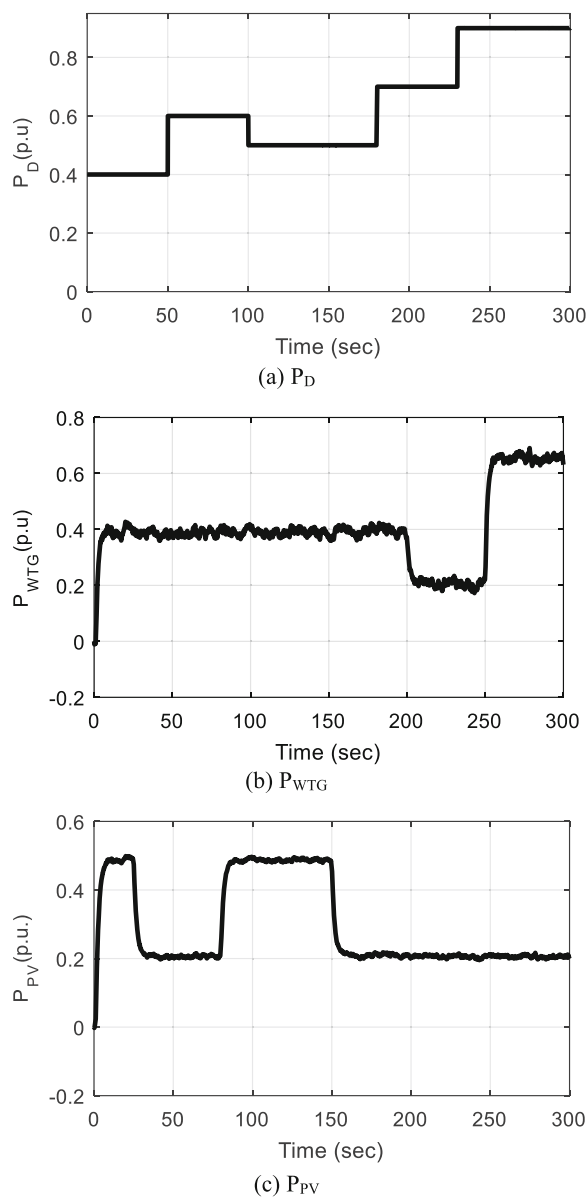


**Fig. 9** Independent load/sources **a**  $P_D$  **b**  $P_{WTG}$  **c**  $P_{PV}$

The percentage of improvements in execution time are shown in Table 6 and Fig. 8 from which it is evident that the SGWO technique offers the remaining two benchmark functions. The SGWO provides more desirable outcome than GWO, GSA, and SCA for  $f_{14}$ . The percentage of improvements in execution time are reported in Table 6 as well as being shown in Fig. 8 from which it is clear that the SGWO technique offers better results with reduced implementation time.

After comparing with different algorithms for unimodal, multimodal and fixed bench mark functions the algorithm is applied to a real engineering problem. The load demand ( $P_D$ ) is varied as shown in Fig. 9 (a). The renewable powers are expressed by (2)–(4) taken from [17] as revealed in Fig. 9 (b) and (c) is applied for real engineering problem which includes distributed power generation system and a two-area test system. Study is performed with PID and AFPID controllers separately. The rule base for AFPID controller is shown in Table 7. The parameters of the suggested controllers are determined using the SGWO approach.

The DPGS frequency is affected by the irregular change of output powers of the PV and WTG, and needs to be controlled by a suitable act of the controllers. Table 8 provides the optimized parameters of the SGWO optimized PID and GWO optimized PID/AFPID. It can be seen that the  $J$  value attained with the execution of the GWO method for the PID controller is 11.95 which is reduced to 10.99 with the SGWO technique. Hence, it proves that the proposed SGWO method provides enhanced results compared to the original GWO technique for tuning the controllers. The suggested AFPID controller further reduces the  $J$  value to 7.774 which shows the dominance of the AFPID over the PID. Here, the SGWO method also gives better results than GWO.

To assess the time-domain response, different cases are tested. In the first case, exclusive change in the load as exposed in Fig. 9 (a) is considered while the solar and wind generations are fixed. For the second case, variations in wind generation and load are introduced as demonstrated in Fig. 9 (a) and (b), while solar generation is kept constant. In the third case, all three  $P_{PV}$ ,  $P_{WTG}$ , and  $P_D$  are varied as shown in Fig. 9. Lastly, robustness investigation is performed to assess the effectiveness of the proposed approach with varied system parameters.

**4.1.1 Case1**

**4.1.1.1 Fluctuation in load with fixed solar and wind power**

This case shows a change in  $P_D$  as shown in Fig. 9 (a) with fixed  $P_{PV}$  and  $P_{WTG}$  of 0.1 p.u and 0.3 p.u, respectively. From the total generation, 0.16 p.u power is fed to

**Table 7** Fuzzy rule base for AFPID

e	NB	NS	Z	PS	PB
de					
NB	NB	NB	NS	NS	Z
NS	NB	NS	NS	Z	PS
Z	NS	NS	Z	PS	PS
PS	NS	Z	PS	PS	PB
PB	Z	PS	PS	PB	PB

**Table 8** SGWO and GWO tuned PID and AFPID parameters

Technique: Controller	Optimized parameters	Objective function value
GWO: PID	$K_p = 1.5531, K_i = 0.1954, K_D = 0.9517$	11.95
SGWO: PID	$K_p = 0.5422, K_i = 0.0801, K_D = 0.0295$	10.99
GWO: AFPID	$K_1 = 0.7148, K_2 = 1.0995$ $K_{P1} = 0.1442, K_{I1} = 0.1701, K_{D1} = 0.6822$ $K_{P2} = 0.1867, K_{I2} = 1.0645, K_{D2} = 1.501$	7.9544
SGWO: AFPID	$K_1 = 0.7163, K_2 = 0.0011$ $K_{P1} = 0.2817, K_{I1} = 0.5591, K_{D1} = 0.5595$ $K_{P2} = 0.2474, K_{I2} = 0.6671, K_{D2} = 0.6676$	7.774

the AE to produce hydrogen gas for the fuel cell which produces a small amount of 0.0002 p.u. Thus, the total generation which can cater to the demand is 0.24 p.u. (As  $P_G = P_{PV} + P_{WTG} + P_{FC} - P_{AE}$ ). Between 50 and 100 s the total demand is 0.6 p.u. as shown in Fig. 9 (a). As the demand exceeds the generation, the power imbalance of 0.35 p.u. is provided by the storage units of FESS, BESS, DEG, and EV. FESS and BESS providing 0.0035 p.u. and 0.001 p.u. as demonstrated in Fig. 10 (c) and (d), respectively. DEG is also connected to the system to provide 0.009 p.u. power while an influential role is played by the EV in supplying the power to the system amounting to 0.34 p.u., shown in Fig. 10 (e) and (f), respectively. The total power from all this storage is around 0.35 p.u. this matches the power required by the system & the frequency is maintained.

During 100–180 s, the  $P_D$  is 0.5 p.u., the renewable power after use for AE is 0.24 p.u., and the fuel cell generates 0.00035 p.u. and the DEG 0.006 p.u. Thus, the total generated power by adding the power of PV, WTG, DEG, and FC is 0.24635 p.u. The deficient power is nearly 0.25365 p.u. and has to be provided by FESS, BESS, and EV. The major part of the deficient power is supplied by the EV which is 0.25 p.u. while FESS releases 0.0028 p.u. and BESS 0.004 p.u. It can similarly be analyzed for the time interval of 180–230 s and 230–300 s.

The frequency deviations and control signals for Case 1 are illustrated in Fig. 10 (a) and (b) from which it is clear that the effectiveness of the AFPID is superior to that of PID. The  $J$  value given by (15) with the SGWO optimized AFPID controller is 10.963 which is less than the 12.621 obtained with the SGWO optimized PID controller. Figure 10 (c)–(f) show the output powers of the different elements of the DPGS system. It can be observed that there is a noteworthy enhancement by the AFPID as the power variation is less with the AFPID controller than with the PID controller.

#### 4.1.2 Case 2

##### 4.1.2.1 Fluctuation in load and wind power having fixed solar generation

In case 2, the  $P_D$  and  $P_{WTG}$  are varied as shown in Fig. 9 (a) and (b) while the  $P_{PV}$  is assumed constant at 0.1 p.u. For the period of 50–100 s, wind power generation is 0.4 p.u. while the AE takes a power of 0.2 p.u. As a result, the power available to meet the demand is 0.3 p.u., while the demand power is 0.6 p.u. during 50–100 s as shown in Fig. 9 (a). Thus, the system needs extra powers of 0.3 p.u. to maintain an equilibrium between generated and demanded power. Figure 11 (c) and (d) show that FESS and BESS supply (shown as negative) powers of 0.003 p.u. and 0.009 p.u., respectively. Power supplied by the DEG is 0.009 p.u. and EV is 0.28 p.u. as demonstrated in Fig. 11 (e) and (f), respectively. During 100–200 s, the load changes from 0.6 p.u. to 0.5 p.u. but the wind remains unchanged. To better visualize the impact the time interval of 200–230 s investigated during which there are variations in both load and wind. The demand power is 0.7 p.u., wind power generation is 0.2 p.u. and PV generation remains at 0.1 p.u.

The total net renewable power including the power consumed by the AE is 0.18 p.u. in this time period, leading to a deficient power of 0.52 p.u. which is catered for by the storage elements. Thus,  $P_{FESS} = 0.005$  p.u.,  $P_{BESS} = 0.015$  p.u.,  $P_{DEG} = 0.0015$  p.u. and  $P_{EV} = 0.5$  p.u. so the total power from the storage units is 0.5215 p.u. Figure 11 (a) displays the frequency variations of the system with both controllers and it is found to be less in the case of AFPID in comparison to the PID controller. The objective function value is decreased to 9.3074 with the proposed SGWO tuned AFPID compared to SGWO optimized PID value of 11.477. The power outputs of BESS, FESS, DEG, and EV are shown in Fig. 11 (c)–(f) and the claimed AFPID controller's better performance in terms of delivering improved system response compared to PID controller can be noted.

#### 4.1.3 Case 3

##### 4.1.3.1 Concurrent fluctuation of load solar and wind power

This is the case in which all the fluctuations are taken into consideration as given in Fig. 9 (a) – (d). The results are shown in Fig. 12.

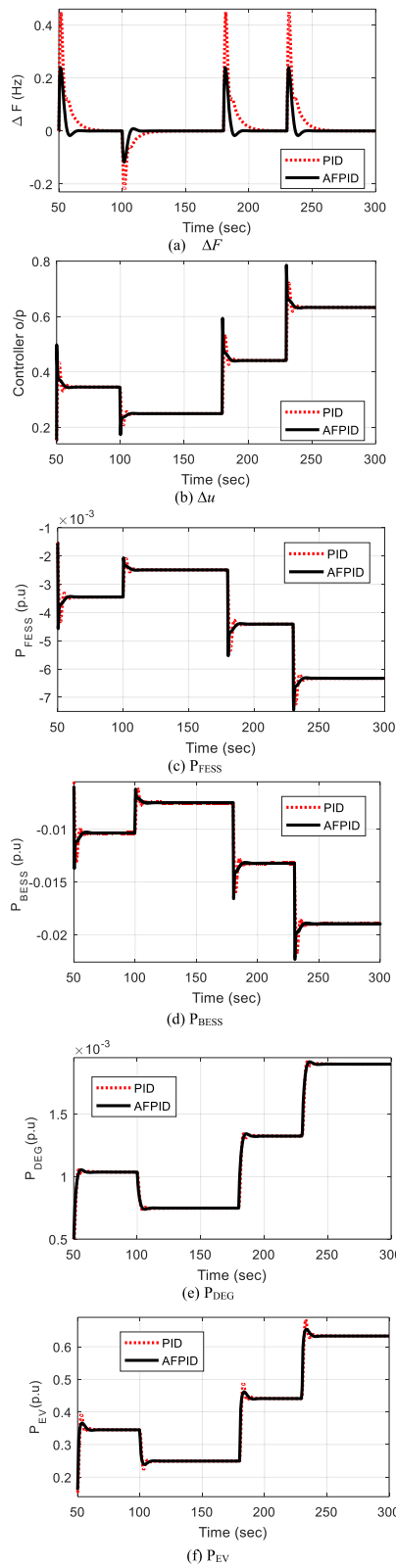


**Fig. 10** System performance for case 1 **a**  $\Delta F$  **b**  $\Delta u$  **c**  $P_{FESS}$  **d**  $P_{BESS}$  **e**  $P_{DEG}$  **f**  $P_{EV}$

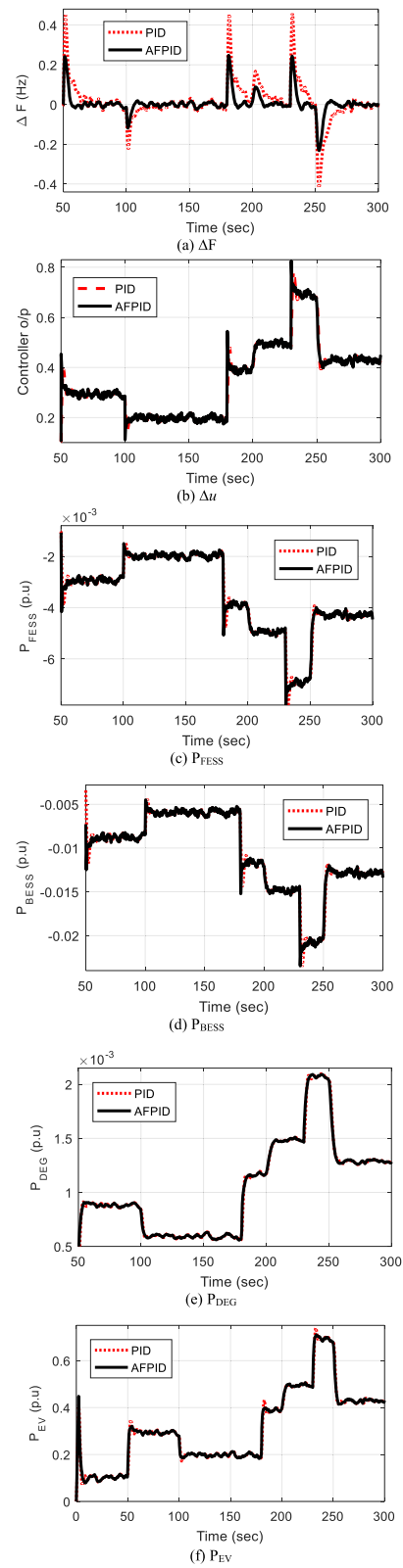


**Fig. 11** System performance for case 2 **a**  $\Delta F$  **b**  $\Delta u$  **c**  $P_{FESS}$  **d**  $P_{BESS}$  **e**  $P_{DEG}$  **f**  $P_{EV}$

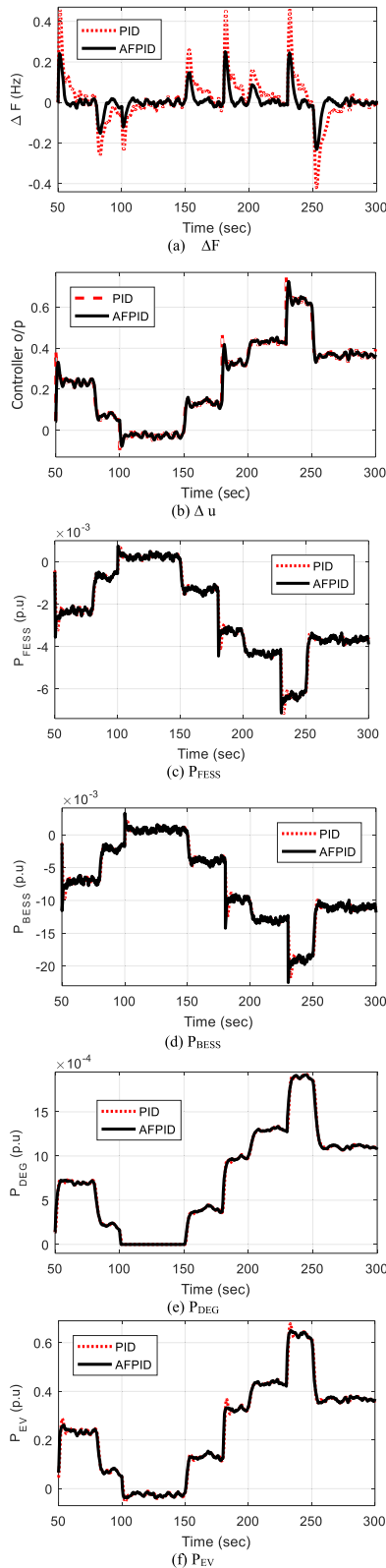


**Fig. 12** System performance for case 3 **a**  $\Delta F$  **b**  $\Delta u$  **c**  $P_{FESS}$  **d**  $P_{BESS}$  **e**  $P_{DEG}$  **f**  $P_{EV}$

**Table 9** Percentage change in  $J$  value under sensitivity analysis

System Parameter	Perturbation	$J$ value	% change
$K_{FESS}$	Increase 70%	7.5708	-2.61
	Decrease 70%	8.0085	3.016
$T_{FESS}$	Increase 90%	7.7855	0.135
	Decrease 90%	7.7659	-0.104
$K_{BESS}$	Increase 70%	7.2254	-7.05
	Decrease 70%	8.5569	10.07
$T_{BESS}$	Increase 90%	7.8078	0.434
	Decrease 90%	7.7631	-0.1402
$M$	Increase 50%	7.0220	-9.67
	Decrease 50%	8.0557	3.62
$D$	Increase 50%	7.5342	-3.084
	Decrease 50%	7.8084	0.44

At  $t = 50$  s, it can be observed from Fig. 9 (a)-(c) that the demand power is 0.6 p.u, the wind power generation is 0.4 p.u, and PV cell generation is 0.2 p.u. AE consumes 0.24p.u from the renewable generation while the fuel cell produces 0.000097 p.u power. The DEG is also connected to the system at  $t = 50$  s to meet the demand and supplies a power of 0.0072 p.u as shown in 12 (e). The total generation less the AE power is thus 0.36729p.u which is 0.23p.u less than the demand. Therefore, the storage units BESS, FESS, and EV provide the deficient power to meet the demand power, i.e.,  $P_{FESS} = 0.0075$ p.u,  $P_{BESS} = 0.0022$ p.u,  $P_{PEV} = 0.23$ p.u as displayed in Fig. 12 (c), (d) (f), respectively. So the total supply power is 0.6070 p.u which matches the demand and the system frequency is stable.

At  $t = 100$  s the  $P_D$  is 0.5 p.u, the  $P_{WTG}$  is 0.4 p.u and  $P_{PV}$  is 0.49 p.u as can be seen from Fig. 9(a) to (c).  $P_{AE}$  and  $P_{FC}$  are 0.356p.u and 0.0014p.u, respectively. As the generation is more than the load the DEG is disconnected, while the storage units FESS and BESS consume 0.0008 p.u and 0.00049 p.u from the system, respectively. EV charges during this period and the power taken is 0.008677 p.u which can be clearly seen from Fig. 12 (e). Thus, the total supplied power is  $P_{renewable} - P_{AE} + P_{FC} + P_{DEG} - (P_{FESS} + P_{BESS} + P_{EV}) = 0.5254$ p.u which matches the demand power.

At  $t = 230$  s, the generation from the renewable sources is 0.4 p.u which is significantly lower than  $P_D$  of 0.9 p.u, as can be visualized from Fig. 9 (a)-(c). As  $P_{AE} = 0.16$ p.u,  $P_{FC} = 0.000066$ p.u, and  $P_{DEG} = 0.0019$ p.u, EV provides most of the power which amounts to 0.64 p.u as seen in Fig. 12 (e) while FESS delivers 0.00072p.u and BESS releases 0.0225 p.u. Thus, the total supply power is 0.905p.u which matches the demand power. Similarly, it can be claimed that with PID and AFPID controllers the power balance is maintained at every instant of time to make the system stable.

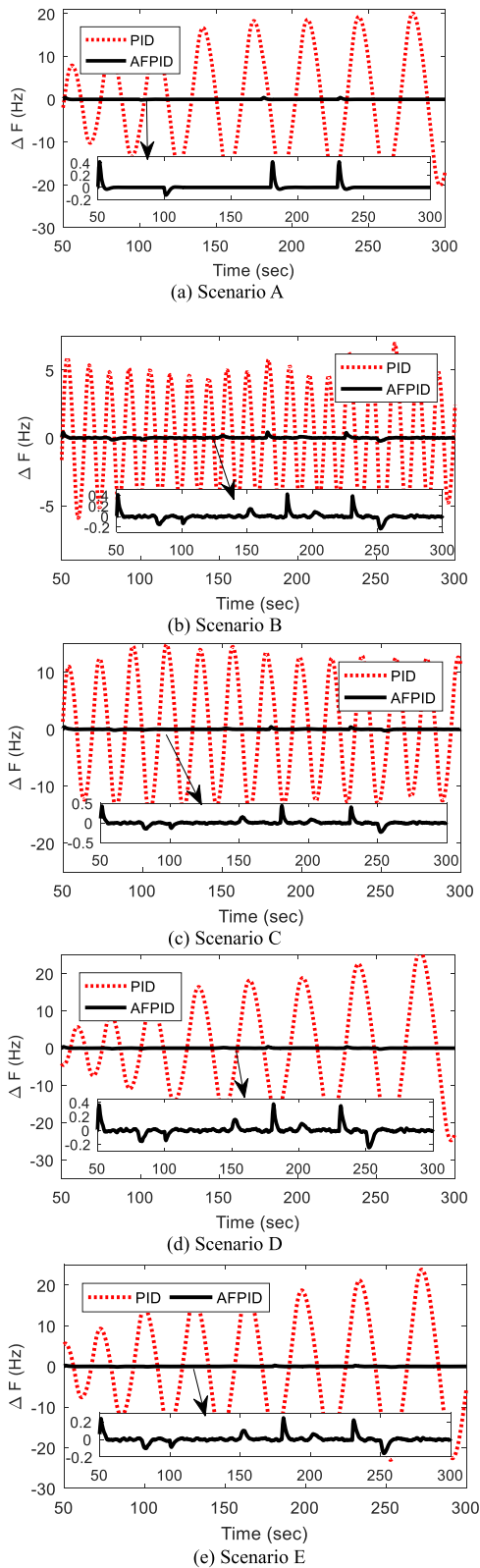


**Fig. 13 a-e** Various Scenarios to show the effect of uncertainty

In case 3, the objective function values with PID and AFPID controller are 10.99 and 7.774, respectively. In all the three cases it is found that SGWO optimized AFPID controller conforms improved system response compared to SGWO optimized PID controller.

**4.1.4 Case 4**

**4.1.4.1 Sensitivity analysis**

The AFPID controller’s flexible nature can be authenticated by considering variability in the variables of the heterogeneous DGPS, such as during unexpected operations due to peculiar changes in environmental conditions. With variations of the power system variables such as  $K_{FESS}$ ,  $T_{FESS}$ ,  $K_{BESS}$ ,  $T_{BESS}$ ,  $M$ , and  $D$ , an alteration in the objective function value ( $J$ ) will be obtained. The percentage change in  $J$  due to the changes in power system variables are compiled in Table 9.

A detailed examination of the outcomes presented in Table 9 shows the advantage of using the AFPID controller in the DPGS system for frequency regulation with noteworthy disparities in the system parameters. Among different parameters of the DPGS system, it is noted that the variations are smaller than 10% for all cases, as shown in Table 9. The flexibility of the proposed SGWO- tuned AFPID for frequency regulation is confirmed in the DPGS system with significant variations in the power system parameters.

**4.1.5 Case 5**

**4.1.5.1 Effect of uncertainty**

For a linear control problem, PID structures are comparatively easy to design and are extensively used. However, the effectiveness of a PID controller may decrease when uncertainty is considered. To demonstrate the dominance of the suggested AFPID, the effectiveness of the AFPID is compared with the PID in various severe situations as presented below:

- Scenario A: Solar and wind powers are not available while EV power and load demand are increased by 40%.
- Scenario B: System inertia constant  $M$  is reduced by 50%
- Scenario C: System inertia constant  $M$  and damping constant  $D$  are both reduced by 50%.
- Scenario D: Time delay is increased by 150 ms.
- Scenario E: EV demand is increased by 50%.

The system frequency deviations for the above scenarios are shown in Fig. 13 (a)-(e). It can be noted that, for all the above scenarios, the frequency oscillates and the system loses its stability with the PID. In contrast, system stability is maintained with the proposed AFPID controller and frequency variations lie within the

**Table 10** Performance table for a two-area thermal power system at  $\Delta P_{D1} = 0.05\text{puMW}$  (5%SLP)

Controller/ Technique	Setting Time ( $T_s$ ) sec			Undershoots ( $U_s$ ) (-ve)			Objective function ITAE $\times 10^{-2}$
	$\Delta F_1$ $\times 10^{-1}$	$\Delta F_2$ $\times 10^{-1}$	$\Delta P_{tie}$ $\times 10^{-1}$	$\Delta F_1$ $\times 10^{-2}$	$\Delta F_2$ $\times 10^{-2}$	$\Delta P_{tie} \times 10^{-2}$	
FPI/PSO [32]	60.7	71.5	56.9	3.89	1.56	0.64	18.27
PID/TLBO [22]	53.3	59.0	33.2	3.07	1.78	0.70	13.47
PIDN/JA [37]	29.7	27.5	25.6	6.00	3.61	1.23	6.86
FPI/(hPSO-PS) [32]	40.7	52.5	40.1	3.55	1.22	0.59	7.99
PI/BFOA [35]	55.2	70.9	63.5	13.12	11.43	4.14	91.56
PI/GA [35]	100.3	100.3	93.7	12.03	10.03	3.57	127.70
PI/(hBFOA-PSO) [36]	73.9	76.5	57.3	12.36	10.42	3.69	58.28
AFPID/(SGWO)	11.8	21.7	14.8	0.97	0.24	0.098	0.32

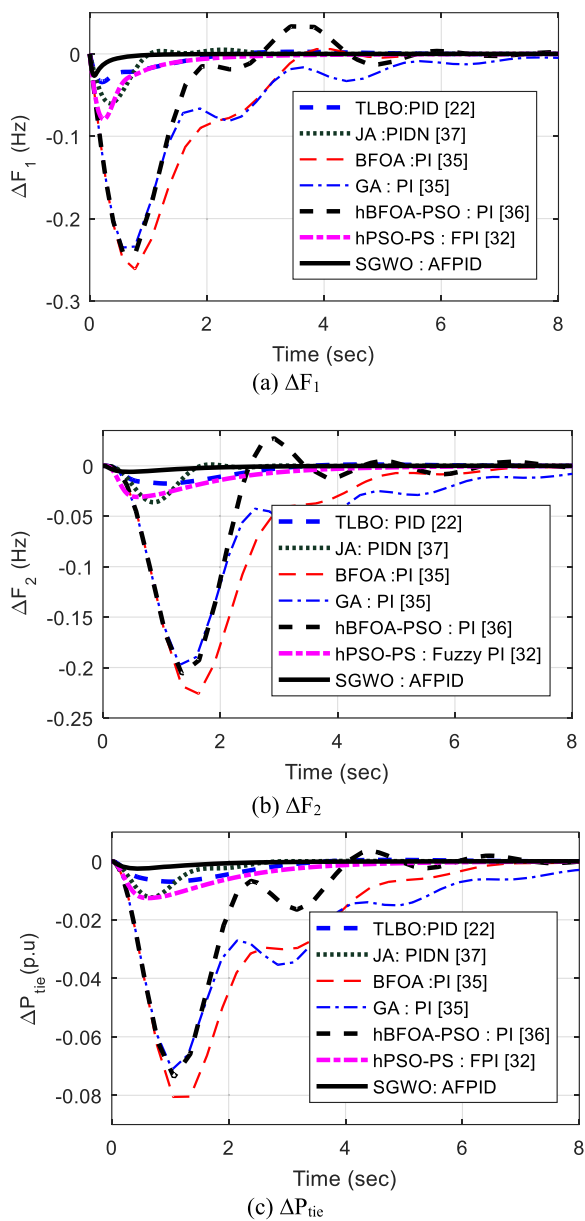


**Fig. 14** System frequency deviation response for two test system **a**  $\Delta F_1$  **b**  $\Delta F_2$  **c**  $\Delta P_{tie}$

tolerance of  $\pm 0.5$  Hz. It is also noted from Fig. 13 (e) that when uncertainty in EV demand is considered, the response with the proposed AFPID is better than the PID controller.

**4.1.6 Case 6**

**4.1.6.1 Comparison with recent AGC technique**

To demonstrate the advantage of the proposed frequency control approach, it is applied to an extensively employed two-area power system [22, 32, 35, 36]. Two similar AFPID controllers are used in each area.

A sudden disturbance of 5% is induced in area 1 at  $t = 0$  s. The SGWO method is used to tune the parameters of the AFPID controller, and its effectiveness is contrasted with some modern optimization techniques such as PSO tuned FPI [32], TLBO tuned PID [22], JA tuned PIDN [37], hPSO-PS tuned FPI [32], BFOA & GA tuned PI [35], and hBFOA-PSO tuned PI [36], and the outcomes are presented in Table 10. The SGWO tuned AFPID parameters are:

$$\begin{aligned}
 K_1 &= 1.9966, K_2 = 0.6527, K_{P1} = 1.9521, K_{I1} \\
 &= 1.9964, K_{D1} = 0.5161, K_{P2} = 1.9948, K_{I2} \\
 &= 1.9968, K_{D2} = 1.5755
 \end{aligned}$$

Table 10 shows that the lowest ITAE value is attained with the modified SGWO- tuned AFPID i.e. lower than the newly proposed frequency control methods. The system responses given in Fig. 14 show that SGWO-tuned AFPID outclasses other automatic generation control methods.

**5 Conclusion**

A Simplified Grey Wolf Optimization (SGWO) algorithm is adopted in this study for the adaptive fuzzy PID controller design for frequency control of a Distributed Power Generation System (DPGS). The proposed SGWO technique is first tested for various unimodal, multi-modal, and fixed dimension functions and values

are compared with the original GWO as well as PSO, GSA, and SCA. It is noted that the SGWO method offers better results than the original GWO in almost all test functions with reduced computational time.

The proposed SGWO method is then used to optimize an AFPID controller for frequency control of the DPGS system. Different nonlinearities such as rate constraints and time delays are included in the system. It is noted that SGWO based AFPID is superior to the conventional PID for frequency regulation under various scenarios. A sensitivity study is also performed to observe the consequence of uncertainties in the system parameters and it is seen that the system performance is satisfactory. The SGWO algorithm is also applied to determine the parameters of the AFPID in a widely used two-area power system and the results obtained demonstrate that the SGWO algorithm-tuned AFPID controller offers a better response than some recently proposed approaches.

## 6 Nomenclature

DPGS: Distributed Power Generation System

PV: Solar Photovoltaic

WTG: Wind Turbine Generator

AE: Aqua Electrolyser

FC: Fuel Cell

DEG: Diesel Engine Generator

FESS: Flywheel Energy Storage System

BESS: Battery Energy Storage System

PEV: Plug in Electric Vehicle

$P_{PV}$ : Power output of PV

$P_{WTG}$ : Power output of WTG

$P_D$ : Load Demand

$P_{FC}$ : Power output of Fuel Cell

$P_{DEG}$ : Power output of DEG

$P_{BESS}$ : Power output of BESS

$P_{FESS}$ : Power output of FESS

$G_{PV}$ : Transfer Function of PV

$K_{PV}$ : Gain of photovoltaic

$T_{PV}$ : Time constant of Photovoltaic

$\eta$ : Conversion Efficiency

$\phi$ : Solar Irradiation

$G_{WTG}$ : Transfer function of WTG

$K_{WTG}$ : Gain of WTG

$T_{WTG}$ : Time constant of WTG

$G_{AE}$ : Transfer Function of AE

$K_{AE}$ : Gain of AE

$T_{AE}$ : Time constant of AE

N: No of units

$G_{FC}$ : Transfer Function of Fuel cell

$K_{FC}$ : Gain of Fuel Cell

$T_{FC}$ : Time Constant of FC

e: Error input to FLC

$G_{BESS}$ : Transfer Function of BESS

$K_{BESS}$ : Gain of BESS

$T_{BESS}$ : Time constant of BESS

$G_{FESS}$ : Transfer function of FESS

$K_{FESS}$ : Gain of FESS

$T_{FESS}$ : Time Constant of FESS

$Y_\alpha, Y_\beta, Y_\delta$ : Current position of  $\alpha, \beta,$  and  $\delta$  wolves

$S_\alpha, S_\beta, S_\delta$ : Updated position of  $\alpha, \beta,$  and  $\delta$  wolves

$G(s)$ : TF of dynamic power system

D: Damping Coefficient

M: Inertia Constant

LFC: Load frequency Control

$\Delta U$ : LFC signal

GWO: Grey Wolf Optimizer

SGWO: Simplified Grey Wolf Optimizer

$\Delta F$ : Frequency Deviation

ISE: Integral Square Error

FLC: Fuzzy logic Controller

NB, NS, Z: Negative Big, Negative small, Zero

PB, PS: Positive Big, Positive Small

de: Change of error input to the FLC

## 7 Appendix

Parameters of investigated system are [17–20].

AE:  $K_{AE} = 0.002, T_{AE} = 0.5$  s,  $T_{FC} = 4.0$  s, FC:  $K_{FC} = 0.01,$   
 PV:  $K_{PV} = 1.0, T_{PV} = 1.8$  s, FESS:  $K_{FESS} = -0.01, T_{FESS} =$   
 $0.1$  s,  $K_n = 0.6,$  WTG:  $K_{WTG} = 1.0, T_{WTG} = 1.0$  s, DEG:  
 $K_{DEG} = 0.003, T_{DEG} = 2.0$  s, BESS:  $K_{BESS} = -0.003, T_{BESS} =$   
 $0.1$  s

### Acknowledgements

Authors would like to thank Veer Surendra Sai University of Technology (VSSUT) Burla for providing necessary research facilities.

### Authors' contributions

Sasmita Padhy has done the modeling of the system with different storage system and plug in electric vehicles and has analyzed their effect on the system with adaptive Fuzzy PID controller. The tuning is done by the Simplified Grey wolf optimization. The simplification is done by Prof. Sidhartha Panda and he has provided all the technical guidance to complete the paper. Both the Authors have read and approved the Final Manuscript.

### Author's information

Sasmita Padhy was born on 29th June 1980 at Ganjam Odisha, India. She obtained her B. Engg (Electrical & Electronics) from National Institute of Science and Technology (NIST) Berhampur Odisha in 2003 and M. Tech (Power System) from BPUT in 2011. Currently She is pursuing Ph. D in VSSUT, Burla and her research interest lies in Power system stability, control and computational intelligence.

Sidhartha Panda is working as a Professor in the Department of Electrical Engineering, Veer Surendra Sai University of Technology (VSSUT), Burla, Sambalpur, Odisha, India. He received Ph.D. degree from Indian Institute of Technology (IIT), Roorkee, India, M.E. degree from Veer Surendra Sai University of Technology (VSSUT). His areas of research include Flexible AC Transmission Systems (FACTS), Power System Stability, Soft computing, Model Order Reduction, Distributed Generation and Wind Energy. Dr. Panda is a Fellow of Institution of Engineers (India).

### Funding

Not applicable.

### Availability of data and materials

Data sharing not applicable to this article as no data were generated or analyzed during the study.

### Competing interests

The authors declare that they have no competing interests.

Received: 19 February 2020 Accepted: 7 January 2021

Published online: 01 February 2021

### References

1. Mirjalili, S., Mirjalili, S. M., & Lewis, A. (2014). Grey wolf optimizer. *Advanced Engineering Software*, 69, 46–61. <https://doi.org/10.1016/j.advengsoft.2013.12.007>.
2. Motlagh, A. C. (2015). Superdefect. Photonic crystal filter optimization using grey wolf optimizer. *IEEE Photonics Technology Letters*, 27, 2355–2358. <https://doi.org/10.1109/LPT.2015.2464332>.
3. Mohanty, S., Subudhi, B., & Ray, P. K. (2016). A new MPPT design using grey wolf optimization technique for photovoltaic system under partial shading conditions. *IEEE Transactions on Sustainable Energy*, 7, 181–188. <https://doi.org/10.1109/TSTE.2015.2482120>.
4. Long, W., Liang, X., Cai, S., Jiao, J., & Zhang, W. (2017). A modified augmented Lagrangian with improved grey wolf optimization to constrained optimization problems. *Neural Computing and Applications*, 28, 421–438. <https://doi.org/10.1007/s00521-016-2357-x>.
5. Padhy, S., Panda, S., & Mahapatra, S. (2017). A modified GWO technique based cascade PI-PD controller for AGC of power systems in presence of plug in electric vehicles. *Engineering Science and Technology, an International Journal*, 20, 427–442. <https://doi.org/10.1016/j.jestch.2017.03.004>.
6. Kohli, M., & Arora, S. (2017). Chaotic grey wolf optimization algorithm for constrained optimization problems. *Journal of Computational Design and Engineering*, Article in press. <https://doi.org/10.1016/j.jcde.2017.02.005>.
7. Yang, B., Zhang, X. S., Yu, T., Sahu, H. C., & Fang, Z. H. (2017). Grouped Grey wolf optimizer for maximum power point tracking of DFIG based wind turbine. *Energy Conversion and Management*, 133, 427–443. <https://doi.org/10.1016/j.enconman.2016.10.062>.
8. Pedersen, M. E. H., & Chipperfield, A. J. (2010). Simplifying particle swarm optimization. *Applied Soft Computing*, 10, 618–628. <https://doi.org/10.1016/j.asoc.2009.08.029>.
9. Panda, S., Sahu, B. K., & Mohanty, P. K. (2012). Design and performance analysis of PID controller for an automatic voltage regulator system using simplified particle swarm optimization. *Journal of the Franklin Institute*, 349, 2609–2625. <https://doi.org/10.1016/j.jfranklin.2012.06.008>.
10. Savino, M. M., Manzini, R., Della, S. V., & Accorsi, R. (2017). A new model for environmental and economic evaluation of renewable energy systems: The case of wind turbines. *Applied Energy*, 189, 739–752. <https://doi.org/10.1016/j.apenergy.2016.11.124>.
11. Jayabarathi, T., Raghunathan, T., Adarsh, B. R., & Suganthan, P. N. (2016). Economic dispatch using hybrid grey wolf optimizer. *Journal of Energy*, 111, 630–641. <https://doi.org/10.1016/j.energy.2016.05.105>.
12. Lee, D. J., & Wang, L. (2008). Small-signal stability analysis of an autonomous hybrid renewable energy power generation/energy storage system part I: Time-domain simulations. *IEEE Transactions on Energy Conversion*, 23, 311–320. <https://doi.org/10.1109/TEC.2007.914309>.
13. Ray, P. K., Mohanty, S. R., & Kishor, N. (2011). Proportional–integral controller based small-signal analysis of hybrid distributed generation systems. *Energy Conversion and Management*, 52(4), 1943–1954. <https://doi.org/10.1016/j.enconman.2010.11.011>.
14. Yilmaz, M., & Krein, P. T. (2013). Review of the impact of vehicle-to-grid technologies on distribution systems and utility interfaces. *IEEE Transactions on Power Electronics*, 28, 5673–5689. <https://doi.org/10.1109/TPEL.2012.2227500>.
15. Yang, H., Chung, Y. C., & Zhao, J. (2013). Application of plug-in electric vehicles to frequency regulation based on distributed signal acquisition via limited communication. *IEEE Transactions on Power Systems*, 28, 1017–1026. <https://doi.org/10.1109/TPWRS.2012.2209902>.
16. Yang, J., Zeng, Z., Tang, Y., Yan, J., He, H., & Wu, Y. (2015). Load frequency control in an isolated micro-grids with electrical vehicle based on multivariable generalised predictive theory. *Energies*, 8, 2145–2163. <https://www.mdpi.com/1996-1073/8/3/2145>.
17. Pan, I., & Das, S. (2011). Fractional order AGC for distributed energy resources using robust optimization. *IEEE Transactions on Smart Grid*, 7, 2175–2186. <https://doi.org/10.1109/TSG.2015.2459766>.
18. Parmar, K. P. S., Majhi, S., & Kothari, D. P. (2012). Load frequency control of a realistic power system with multi-source power generation. *International Journal of Electrical Power & Energy Systems*, 42, 426–433. <https://doi.org/10.1016/j.ijepes.2012.04.040>.
19. Golpira, H., Bevrani, H., & Golpira, H. (2011). Application of GA optimization for automatic generation control design in an interconnected power system. *Energy Conversion and Management*, 52, 2247–2255. <https://doi.org/10.1016/j.enconman.2011.01.010>.
20. Pan, I., & Das, S. (2016). Fractional order fuzzy control of hybrid power system with renewable generation using chaotic PSO. *ISA Transactions*, 62, 19–29. <https://doi.org/10.1016/j.isatra.2015.03.003>.
21. Mohanty, B., Panda, S., & Hotta, P. K. (2014). Controller parameters tuning of differential evolution algorithm and its application to load frequency control of multisource power system. *International Journal of Electrical Power Energy System*, 54, 77–85. <https://doi.org/10.1016/j.ijepes.2013.06.029>.
22. Sahu, R. K., Panda, S., Rout, U. K., & Sahoo, D. K. (2016). Teaching learning based optimization algorithm for automatic generation control of power system using 2-DOFPID controller. *International Journal of Electrical Power Energy System*, 77, 67–77. <https://doi.org/10.1016/j.ijepes.2015.11.082>.
23. Sahu, R. K., Panda, S., & Padhan, S. (2014). Optimal gravitational search algorithm for interconnected power systems. *Ain Shams Engineering Journal*, 5, 721–733. <https://doi.org/10.1016/j.asej.2014.02.004>.
24. Abd, A. Y., & Ali, S. E. (2015). Cuckoo search algorithm based load frequency controller design for nonlinear inter connected power system. *International Journal of Electrical Power Energy System*, 73, 632–643. <https://doi.org/10.1016/j.ijepes.2015.05.050>.
25. Abd, S. M., Elazim, E., & Ali, S. (2016). Load frequency controller design via BAT algorithm for nonlinear inter connected power system. *International Journal of Electrical Power Energy System*, 77, 166–177. <https://doi.org/10.1016/j.ijepes.2015.11.029>.
26. Khadanga, R. K., Kumar, A., & Panda, S. (2019). A novel modified whale optimization algorithm for load frequency controller design of a two area power system composing of PV grid and thermal generator. *Neural computing & application*. <https://doi.org/10.1007/s00521-019-04321-7>.
27. Mirjalili, S. (2016). SCA a sine cosine algorithm for solving optimization problems. *Knowledge Based Systems*, 96, 120–133. <https://doi.org/10.1016/j.knsys.2015.12.022>.
28. Annamraju, A., & Nandiraju, S. (2019). Coordinated control of conventional power sources and PHEVs using Jaya algorithm optimized PID controller for frequency control of a renewable penetrated power system. *Protection and Control of Modern Power Systems*, 4, 28. <https://doi.org/10.1186/s41601-018-0144-2>.
29. Dahab, Y. A., Abubkar, H., & Tarek Hassan, M. (2020). Adaptive load frequency control of power systems using electro-search optimization supported by balloon effect. *IEEE ACCESS*. <https://doi.org/10.1109/ACCESS.2020.2964104>.
30. Mahapatra, T. K., Dey, A. K., & Sahu, B. K. (2015). Implementation of SSA based two degree of freedom fractional order PID controller for AGC with diverse source of generation. *International Journal of Recent Technology and Engineering*, 7, 346–356.
31. Sudha, K. R., Raju, Y. B., Sekhar, A. C. (2012). Fuzzy C-means clustering for robust decentralized load frequency control of interconnected power system with generation rate constraint. *International Journal of Electrical Power and Energy Systems*, 37, 58–66. <https://doi.org/10.1016/j.ijepes.2011.12.005>.
32. Sahu, R. K., Panda, S., & Sekher, G. T. C. (2015). A novel hybrid PSO-PS optimized fuzzy PI controller for AGC in multi area interconnected power systems. *International Journal of Electrical Power Energy System*, 64, 880–893. <https://doi.org/10.1016/j.ijepes.2014.08.021>.
33. Fereidouni, A., Masoum, A. S., & Moghbel, M. (2015). A new adaptive configuration of PID type fuzzy logic controller. *ISA Trans*, 56, 222–240. <https://doi.org/10.1016/j.isatra.2014.11.010>.
34. Mohanty, D., & Panda, S. (2020). Frequency control of hybrid power system by sine function adapted improved whale optimisation technique. *International Journal of Ambient Energy*. <https://doi.org/10.1080/01430750.2020.1839550>.
35. Ali, E. S., & Abd-Elazim, S. M. (2011). Bacteria foraging optimization algorithm based loadfrequency controller for interconnected power system. *International Journal of Electrical Power Energy System*, 33, 633–638. <https://doi.org/10.1016/j.ijepes.2010.12.022>.
36. Panda, S., Mohanty, B., & Hota, P. K. (2013). Hybrid BFOA-PSO algorithm for automatic generation control of linear and nonlinear interconnected power systems. *Applied Soft Computing*, 13, 4718–4730. <https://doi.org/10.1016/j.asoc.2013.07.021>.
37. Singh, S. P., Prakash, T., Singh, V. P., & Babu, M. G. (2017). Analytic hierarchy process based automatic generation control of multi area interconnected power system using jaya algorithm. *Engineering Applications of Artificial Intelligence*, 60, 35–44.